Numerically probing the universal operator growth hypothesis

Robin Heveling,* Jiaozi Wang,† and Jochen Gemmer‡
Department of Physics, University of Osnabrück, D-49076 Osnabrück, Germany

(Received 29 March 2022; accepted 8 July 2022; published 29 July 2022)

Recently, a hypothesis on the complexity growth of unitarily evolving operators was presented. This hypothesis states that in generic, nonintegrable many-body systems, the so-called Lanczos coefficients associated with an autocorrelation function grow asymptotically linear, with a logarithmic correction in one-dimensional systems. In contrast, the growth is expected to be slower in integrable or free models. In this paper, we numerically test this hypothesis for a variety of exemplary systems, including one-dimensional and two-dimensional Ising models as well as one-dimensional Heisenberg models. While we find the hypothesis to be practically fulfilled for all considered Ising models, the onset of the hypothesized universal behavior could not be observed in the attainable numerical data for the Heisenberg model. The proposed linear bound on operator growth associated with the hypothesis eventually stems from geometric arguments involving the locality of the Hamiltonian as well as the lattice configuration. We derive and investigate a related geometric bound, and we find that while the bound itself is not sharply achieved for any considered model, the hypothesis is nonetheless fulfilled in most cases.

DOI: 10.1103/PhysRevE.106.014152

I. INTRODUCTION

The issue of the emergence of irreversible behavior from the unitary time evolution of quantum mechanics has yet to be answered in a satisfying manner [1]. In this context, concepts like the "eigenstate thermalization hypothesis" [2–4] and "quantum typicality" [5–7] have been introduced as possible fundamental mechanisms behind an eventual equilibration of isolated quantum systems. The idea of typicality is that an overwhelming majority of pure states (at some energy) give rise to corresponding thermal expectation values. Thus, it is quite likely that over the course of time, a pure state eventually ends up in the giant "bubble" of typical states, signaling an apparent equilibration of the system. In the Heisenberg picture formulation of quantum mechanics, it is not the states that are time-dependent, but rather the observables themselves. Hence, it may be somewhat expected to find a similar notion of typicality for observables, going from initially simple, few-particle operators to more complex, generic operators. Recent works have studied this notion of operator growth from various angles [8–13].

In this paper, we refer to the particular work presented in Ref. [14], in which a hypothesis on the universality of operator growth is brought forth. Said hypothesis is formulated in the framework of the *recursion method* [15,16], and it makes a statement about the growth of the so-called Lanczos coefficients, real numbers that characterize the complexity growth of operators over the course of time. In the following, we numerically test this operator growth hypothesis for various models and observables. Similar numerical investigations have been conducted [17,18].

The paper at hand is organized as follows: we briefly restate the universal operator growth hypothesis and introduce related quantities in Sec. II. Following that, in Sec. III we derive an upper bound on the complexity growth of operators based on geometric arguments. We present our numerical results and relate them to the operator growth hypothesis in Sec. IV. We summarize our main results and conclude in Sec. V.

II. OPERATOR GROWTH HYPOTHESIS

For self-containedness, in this section we restate the operator growth hypothesis brought forward in Ref. [14]. To start, the main quantities that eventually play a role in the hypothesis are introduced. We consider a system in the thermodynamic limit described by a local Hamiltonian $\mathcal{H}$ [here, local means short-range, few-body interactions]. An observable of interest represented by a Hermitian operator O gives rise to a corresponding autocorrelation function

$$C(t) = \mathrm{Tr}[O(t)O], \tag{1}$$

where $O(t) = e^{\mathrm{i}\mathcal{H}t} O e^{-\mathrm{i}\mathcal{H}t}$ is the time-dependent operator in the Heisenberg picture ($\hbar = 1$). In the following, it is convenient to work directly in the Hilbert space of operators and denote its elements O as states $|O)$. This Hilbert space of operators is equipped with an inner product $(O_1|O_2) = \mathrm{Tr}[O_1^\dagger O_2]$, which induces a norm via $||O|| = \sqrt{(O|O)}$. The Liouvillian superoperator is defined by $\mathcal{L}|O) = [\mathcal{H}, O]$ and propagates a state $|O)$ in time such that the autocorrelation function may be written as $C(t) = (O|e^{i\mathcal{L}t}|O)$.

The *Lanczos algorithm* can be employed to calculate a tridiagonal representation of the Liouvillian $\mathcal{L}$ in a (finite)

*rheveling@uos.de
†jiaowang@uos.de
‡jgemmer@uos.de

 ©2022 American Physical Society

subspace determined by some "seed" observable O. To start the iterative scheme detailed below, we take the normalized initial state $|O_0) = |O)$, i.e., $(O|O) = 1$, and set $b_1 = ||\mathcal{L}O_0||$ as well as $|O_1) = \mathcal{L}|O_0)/b_1$. Then we iteratively compute

$$\begin{aligned} |\mathcal{Q}_n) &= \mathcal{L}|O_{n-1}) - b_{n-1}|O_{n-2}), \\ b_n &= ||\mathcal{Q}_n||, \\ |O_n) &= |\mathcal{Q}_n)/b_n. \end{aligned} \tag{2}$$

The tridiagonal representation of the Liouvillian in the *Krylov basis* $\{|O_n)\}$ is then given by

$$L_{mn} = (O_m|\mathcal{L}|O_n) = \begin{pmatrix} 0 & b_1 & 0 & \cdots \\ b_1 & 0 & b_2 & \\ 0 & b_2 & 0 & \ddots \\ \vdots & & \ddots & \ddots \end{pmatrix}_{mn}, \tag{3}$$

where the *Lanczos coefficients* b_n are real, positive numbers output by the algorithm. They can be interpreted as hopping amplitudes in a tight-binding model, and their iterative computation is an elementary part of the recursion method [15,16].

Before the hypothesis itself is stated, we will briefly present the relation between the Lanczos coefficients b_n and the autocorrelation function $C(t)$ or, respectively, its Fourier transform, the spectral function

$$\Phi(\omega) = \int_{-\infty}^{\infty} e^{-i\omega t}\, C(t)\, dt. \tag{4}$$

There exists a (nonlinear) one-to-one map between the Lanczos coefficients b_n and the spectral function $\Phi(\omega)$, thus a set of b_n's uniquely determines $\Phi(\omega)$ and vice versa. It can be shown that the Lanczos coefficients b_n appear in the continued fraction expansion of $\Phi(\omega)$, i.e.,

$$\Phi(\omega) = \mathrm{Re}\, \cfrac{2}{i\omega + \cfrac{b_1^2}{i\omega + \cfrac{b_2^2}{i\omega + \cdots}}}. \tag{5}$$

The universal operator growth hypothesis brought forward in Ref. [14] concerns the asymptotic behavior of the Lanczos coefficients b_n. The hypothesis can informally be stated as follows: The Lanczos coefficients b_n should "grow as fast as possible" in generic, nonintegrable systems. It turns out that (as detailed below) the fastest possible growth rate is (asymptotically) linear, i.e.,

$$b_n \sim \alpha n + \gamma + o(1) \tag{6}$$

for some real constants $\alpha > 0$ and γ. In the special case of a one-dimensional system, the fastest possible growth is sublinear due to an additional logarithmic correction, i.e.,

$$b_n \sim A\, \frac{n}{\ln n} + o(n/\ln n), \tag{7}$$

where $A > 0$ is a real constant and $o(g_n)$ denotes some real sequence f_n with $\lim_{n\to\infty} |f_n/g_n| = 0$.

These bounds on the fastest possible (asymptotic) growth eventually originate from a powerful statement on the behavior of the spectral function $\Phi(\omega)$ for large ω. The spectral function usually features nonvanishing high-frequency tails for generic many-body systems. By means of geometric arguments, these tails can be rigorously bounded by an exponential function such that

$$\Phi(\omega) \leqslant K e^{-\kappa|\omega|} \tag{8}$$

for some adequately chosen constant $K > 0$ and decay constant $\kappa > 0$, which is related to the geometry of the system [19]. It can be shown that spectral functions actually featuring exponentially decaying tails give rise to asymptotically linear growth in the Lanczos coefficients [20,21]. Therefore, the operator growth hypothesis is equivalent to an exponentially decaying spectral function, and it basically states that the Lanczos coefficients should grow as fast as "permitted by the geometry." There are a few examples for which linear growth is analytically known to be achieved [14,22].

III. BOUND ON GROWTH VIA MOMENTS

The asymptotically linear bound on the growth of b_n or, respectively, the exponential bound on the decay of the spectral function $\Phi(\omega)$ are ultimately a consequence of geometric arguments concerning the locality of the Hamiltonian and the observable as well as the specific lattice geometry of the system [19].

A straightforward way to apply these arguments is by considering the moments μ_{2n} of the autocorrelation function and determining an upper bound by taking the respective system geometry into account. The moments of the autocorrelation function $C(t)$ are defined by

$$\mu_{2n} = \frac{d^{2n}}{dt^{2n}} C(t)\Big|_{t=0} \tag{9}$$

or, respectively, in terms of the spectral function

$$\mu_{2n} = \int \omega^{2n}\, \Phi(\omega)\, d\omega. \tag{10}$$

Since $C(t)$ is an even function, all odd moments necessarily vanish. The information contained in the moments μ_{2n} is identical to the information conveyed by the Lanczos coefficients b_n. It is detailed in Appendix how to translate between the two quantities.

Employing the Heisenberg equation of motion for time-dependent operators, Eq. (9) can be written as

$$\mu_{2n} = ||\mathcal{L}^n O||^2. \tag{11}$$

This quantity will be bounded from above in the following. We again consider a local operator O with $||O|| = 1$ and a local Hamiltonian $\mathcal{H} = \sum_\ell h_\ell$ with local terms h_ℓ or, respectively, a local Liouvillian $\mathcal{L} = \sum_k \ell_k$ with local terms $\ell_k = [h_k, \cdot\,]$.

The norm of a local Liouvillian ℓ (we assume periodicity such that all ℓ_k are of the same type) applied to some operator $\mathcal{A}$ can be bounded by

$$||\ell\mathcal{A}|| \leqslant \mathcal{E}\, ||\mathcal{A}||, \tag{12}$$

where $\mathcal{E} = E_{\max} - E_{\min}$ denotes the maximum eigenvalue of ℓ, and $E_{\max}$ ($E_{\min}$) is the maximum (minimum) eigenvalue of h. The equality holds if the operator $\mathcal{A}$ is an eigenoperator of the local Liouvillian corresponding to the largest eigenvalue. Utilizing the triangle inequality and iteratively applying

Eq. (12) yields

$$\begin{aligned} ||\mathcal{L}^n O|| &= || \sum_{k_1,\ldots,k_n} \ell_{k_n} \cdots \ell_{k_1} O|| \\ &\leqslant \sum_{k_1,\ldots,k_n} ||\ell_{k_n} \cdots \ell_{k_1} O|| \\ &\leqslant \sum_{k_1,\ldots,k_n} \mathcal{E}^n = \mathcal{E}^n N_{\text{sum}}(n), \end{aligned} \tag{13}$$

where N_{sum} denotes the number of terms in the sum (it is specified below which terms are actually counted). This number typically grows quite fast with n and can be exactly determined for simple geometries, as is presented at the end of this section. Consequently, the moments can be bounded as

$$\mu_{2n} = ||\mathcal{L}^n O||^2 \leqslant \mathcal{E}^{2n} N_{\text{sum}}^2(n). \tag{14}$$

Regarding the former results, it can be noted that the above bound is tighter than similar bounds brought forth in Ref. [14]. For instance, $\mathcal{E}^{2n} N_{\text{sum}}^2(n) < (2\mathcal{E}')^{2n} P_n^2$, where the right-hand side refers to the bound corresponding to asymptotically linear growth presented in Appendix F of Ref. [14]. For more details, see also Ref. [26].

The fastest possible growing moments, i.e., moments equal to the right-hand side of Eq. (14), can be translated to corresponding Lanczos coefficients as described in Appendix. For later reference, we denote the coefficients obtained in this way by $\mathcal{B}_n$. They depend on the energy scale $\mathcal{E}$ as well as on the lattice geometry expressed through N_{sum}. Both quantities are exactly known for the models studied below. Even though Eq. (14) gives a rigorous upper bound on the moments, the $\mathcal{B}_n$ obtained from this bound do not necessarily constitute a pointwise upper bound on b_n. In Sec. IV A, we give more details on the interpretation of the coefficients $\mathcal{B}_n$.

To end this section, we determine the number N_{sum} for the simple case of a one-dimensional chain with nearest-neighbor interactions, i.e., $\mathcal{H} = \sum_\ell h_{\ell,\ell+1}$. We start with a local operator O whose support is only on-site zero (the support of an operator contains all sites on which the operator is not equal to the identity, e.g., here $O = \cdots \otimes I \otimes O_0 \otimes I \otimes \cdots$, where I denotes the identity on a given site).

The operator $\mathcal{L}O$ consists of operators $\ell_{-1,0} O_0$ with support on sites $(-1, 0)$ as well as $\ell_{0,1} O_0$ with support on sites (0,1). Next, $\mathcal{L}^2 O$ contains six operators with support on sites $(-2, -1, 0)$, $(-1, 0)$, $(-1, 0, 1)$, $(-1, 0, 1)$, (0,1), and (0,1,2), respectively. In these lists, we include (and count) trivially nonvanishing operators, i.e., operators that vanish due to a lack of overlap between respective supports are not counted (for example, the operator $\ell_{8,9} O_0$ trivially vanishes), however operators with respective overlap between supports (like $\ell_{0,1} O_0$) are always counted, even though the operator may vanish due to the specific choice of the local Hamiltonian and initial observable. In this manner, we iteratively apply the Liouvillian to the initial operator, grow the supports accordingly, and keep track of the number of potentially nonvanishing operators. For the case at hand, the above procedure gives rise to a sequence of numbers $N_{\text{sum}}(n) = 1, 2, 6, 22, 94, 454, 2430, 14\,214, \ldots$ of terms in the sum in Eq. (14). As rigorously shown in Ref. [23], there exists a closed mathematical expression for this sequence, i.e., $N_{\text{sum}}(n) = B_n(2)$, where B_n denote the Bell polynomials.

The above strategy of counting terms (which is presented in Ref. [23] in a more rigorous way) in principle also works for more complicated geometries, e.g., higher-dimensional or with long-range interactions. However, it can be quite involved to keep track of all contributions, and closed expressions such as the one above are generally difficult to come by. Thus, for the lattice geometries investigated below, i.e., with next-nearest-neighbor and two-dimensional interactions, respectively, we compute the sequences iteratively up to some n.

IV. NUMERICAL ANALYSIS

In this section, we numerically check the proposed operator growth hypothesis by explicitly calculating the Lanczos coefficients b_n for various exemplary setups. These setups include one-dimensional (1D) and two-dimensional (2D) Ising models as well as 1D Heisenberg models, all paired with a variety of different observables. We compare the calculated b_n with the coefficients $\mathcal{B}_n$ [obtained from the right-hand side of Eq. (14)] by explicitly calculating $\mathcal{E}$ and N_{sum} for each model.

In practice, it is only possible (for the considered systems at least) to obtain a finite number N of Lanczos coefficients b_n, since the dimension of the operator space grows exponentially. The achievable number of coefficients N is around 30 for the 1D Ising model and around 15 for the Heisenberg model. The difference in obtainable b_n is due to the fact that the operator space grows much faster for the Heisenberg model than for the Ising model. For all considered systems, the Hamiltonian $\mathcal{H}$ consist of two terms, an integrable part $\mathcal{H}_0$ and an integrability-breaking part $\mathcal{V}$, i.e.,

$$\mathcal{H} = \mathcal{H}_0 + \lambda \mathcal{V} \tag{15}$$

(except for the 2D Ising model, where $\mathcal{H}_0$ is already nonintegrable). The parameter λ tunes the nonintegrability of the model. We suppose that the total Hamiltonian $\mathcal{H}$ (as well as $\mathcal{H}_0$ and $\mathcal{V}$ individually) can be written in terms of local Hamiltonians, i.e., $\mathcal{H} = \sum_\ell h_\ell$. Again, the local terms usually describe short-range, few-body interactions. For each model, we consider a number of observables O. Importantly, all observables should have zero overlap with any conserved quantity [24], for example, $(O|\mathcal{H}) = 0$.

A. Transverse Ising model

The first model under consideration is a transverse Ising model with a tilted field. Respective unperturbed and total Hamiltonians are given by

$$\begin{aligned} \mathcal{H}_0 &= \sum_\ell J_{xx} \sigma_\ell^x \sigma_{\ell+1}^x + B_z \sigma_\ell^z, \\ \mathcal{H} &= \mathcal{H}_0 + B_x \sum_\ell \sigma_\ell^x, \end{aligned} \tag{16}$$

where $\sigma_\ell^{x,y,z}$ denote Pauli operators on site ℓ. The magnetic field B_x in the x-direction plays the role of the integrability-breaking parameter λ in Eq. (15), i.e., the system is nonintegrable for $B_x \neq 0$ and integrable for $B_x = 0$. We set $J_{xx} = 1.0$ and $B_z = -1.05$ and calculate the Lanczos

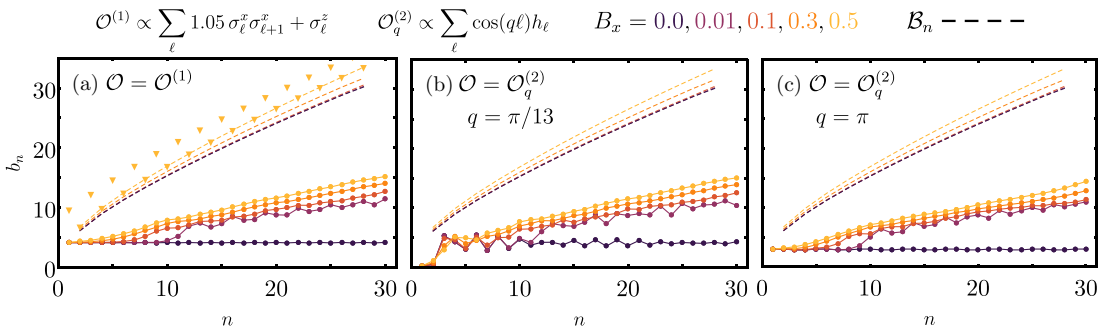

FIG. 1. Lanczos coefficients b_n of the transverse Ising model for the 2-local observables (a) $O^{(1)}$, (b) slow mode of $O^{(2)}_q$ with $q = \pi/13$, and (c) fast mode of $O^{(2)}_q$ with $q = \pi$. The integrability-breaking magnetic field attains values from $B_x = 0.0$ to 0.5. For all observables, the transition from a free model to a nonintegrable model is evident. The coefficients $\mathcal{B}_n$ are explicitly depicted in (a) for the case $B_x = 0.5$ as yellow triangles. Dashed lines indicate the "lower branches" of the corresponding $\mathcal{B}_n$. To avoid clutter, only the dashed lines are depicted as a guide to the eye for other values of B_x and in all subsequent figures. The coefficients $\mathcal{B}_n$ are larger than the physical b_n by a factor of about 2 for all observables.

coefficients for various observables as detailed in Sec. II. In practice, it is convenient to adopt the set of Pauli strings as a working basis of the Hilbert space of operators [14,25].

The behavior of the Lanczos coefficients during a transition from an integrable to a nonintegrable 1D Ising model has been systematically probed in Ref. [17] for local observables supported on one or two sites. Thus, here, we primarily focus on observables with support throughout the whole system. As a first example, we consider the 2-local observable

$$O^{(1)} \propto \sum_\ell 1.05\,\sigma^x_\ell\sigma^x_{\ell+1} + \sigma^z_\ell, \tag{17}$$

where 2-local means that the local terms are supported on two sites, respectively. The choice of the parameter 1.05 in front of the xx-coupling term ensures that $(O^{(1)}|\mathcal{H}) = 0$. This exact setup was also studied in Ref. [14]. The corresponding Lanczos coefficients are depicted in Fig. 1(a) for various values of the integrability-breaking parameter B_x.

The Hamiltonian of the bare transverse Ising model (with $B_x = 0$) can be mapped onto free fermions via a Jordan-Wigner transformation. Further, the observable in Eq. (17) is local in the fermionic picture. In this noninteracting case, the Lanczos coefficients seem to be more or less constant. As soon as a small perturbation that breaks the integrability is introduced, e.g., $B_x = 0.01$, the Lanczos coefficients begin to grow. The distinction between the free case and nonintegrable cases is clearly visible in Fig. 1(a). The growth of the Lanczos coefficients for larger values of B_x already looks quite linear. A possible logarithmic correction due to the system's one-dimensionality is not directly noticeable in the data, although it has been observed in this model [17].

Before we continue, we want to make some remarks on the interpretation of the coefficients $\mathcal{B}_n$. As mentioned, the $\mathcal{B}_n$ are computed by assuming that the moments grow as fast as possible, i.e., an equality sign in Eq. (14), and translating these maximum moments to Lanczos coefficients as detailed in Appendix. However, even though Eq. (14) gives a rigorous upper bound on the moments, the resulting $\mathcal{B}_n$ do not necessarily constitute a strict pointwise upper bound on the b_n (this is simply due to the way the Lanczos coefficients are calculated from the moments). Thus, the $\mathcal{B}_n$ should not be thought of as such. Rather, the $\mathcal{B}_n$ represent a sort of "global uniform" upper bound, meaning that it is impossible to further increase the value of one specific coefficient "by hand" without simultaneously decreasing the value of another one (or several other ones). In this sense, the $\mathcal{B}_n$ are the "maximum" coefficients. If the "physical" coefficients b_n followed the $\mathcal{B}_n$ tightly, then one could indeed conclude that the upper bound in Eq. (14) was sharply achieved and that the Lanczos coefficients would indeed grow "as fast as possible," given the constraints in Eqs. (12) and (13).

The values of the $\mathcal{B}_n$ are explicitly depicted in Fig. 1(a) for $B_x = 0.5$. The coefficients clearly exhibit some even-odd effects. These even-odd effects also occur for all other considered parameters and models. To avoid clutter, we only show the "lower branches" of the $\mathcal{B}_n$ as dashed lines for smaller values of B_x. Therefore, the dashed lines in Fig. 1(a) (and all subsequent figures) serve as a guide to the eye for the "maximal possible" coefficients $\mathcal{B}_n$. The energy scale is $\mathcal{E} = 3.2$ (for $B_x = 0.5$), and N_{sum} is obtained as detailed at the end of Sec. III, with the important difference that the initial operator is now supported on two sites. In Fig. 1(a), it is evident that the coefficients $\mathcal{B}_n$ are larger than the physical coefficients b_n by about a factor of 2. Thus, the upper bound on the moments is not sharply achieved, i.e., Eq. (14) is an overestimate [26].

This general behavior of the b_n as well as the $\mathcal{B}_n$ is reproduced for the next observable, which constitutes an energy density wave with momentum q, i.e.,

$$O^{(2)}_q \propto \sum_\ell \cos(q\ell)h_\ell. \tag{18}$$

We study a relatively slow dynamic with $q = \pi/13$ and a relatively fast dynamic with $q = \pi$. Both observables are local in the fermionic picture. The Lanczos coefficients b_n and coefficients $\mathcal{B}_n$ are depicted in Fig. 1(b) for $q = \pi/13$ and in Fig. 1(c) for $q = \pi$. In both cases, the qualitative behavior is quite similar to the first observable. Again, the Lanczos coefficients of the free model with $B_x = 0$ seem to be more or less constant. Once the additional magnetic field is added, the model becomes nonintegrable, and at some point the b_n grow approximately linearly. Just as for the first observable, the derived bounds are not tight and the $\mathcal{B}_n$ are larger by a factor of about 2.

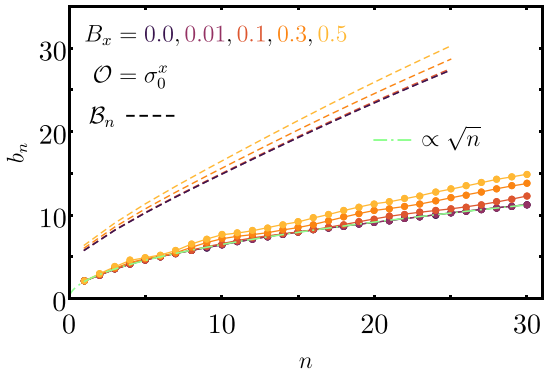

FIG. 2. Lanczos coefficients b_n of the transverse Ising model for a local observable $O^{(3)} = \sigma_0^x$ for various integrability-breaking parameters B_x. The distinction between the free and nonintegrable curves is not as striking as before. The green dash-dotted line indicates a fit $\propto \sqrt{n}$ to the data of the integrable model. Dashed lines serve as a guide to the eye for the coefficients $\mathcal{B}_n$, which are larger by a factor of about 2.

The final considered observable for the one-dimensional Ising model is a local operator whose support only contains a single site, i.e.,

$$O^{(3)} = \sigma_0^x. \tag{19}$$

The corresponding Lanczos coefficients are depicted in Fig. 2. There is a clear qualitative difference compared to the observables investigated thus far. For the free case with $B_x = 0$, the Lanczos coefficients seem to no longer be bounded by a constant. Rather, the growth is quite accurately described by a square-root $\propto \sqrt{n}$ (see the fit). For this particular model and observable, the square-root-like growth can be understood analytically [22]. Further, this kind of growth has been observed for a variety of other integrable models [14,16,27]. We suspect that this qualitatively different behavior compared to the previous cases is due to the specific choice of the observable, which is, in contrast to all previously considered observables, nonlocal in the fermionic picture. Consequently, one could be inclined to formulate two sufficient conditions, which both have to be met in order for the b_n to be bounded by a constant. First, the Hamiltonian has to describe a free model, and second, the observable has to be local. For the observable at hand, which is nonlocal in the fermionic picture, the second condition is violated. Therefore, the Lanczos coefficients are not bounded by a constant, rather they grow as a square root.

As the Hamiltonian departs from the integrable/free point once $B_x \neq 0$, the b_n grow faster (which is not too surprising, since there are simply more terms in the Hamiltonian). From the computed data it is not immediately obvious whether the growth becomes linear (with a logarithmic correction) or remains more or less square-root-like. Possibly, the data for larger B_x in Fig. 2 hint at an onset of linear growth for larger n. However, the distinction is certainly not as clear as for the local observables. Again, the $\mathcal{B}_n$ are off by a factor of about 2.

It is interesting to note that in the nonintegrable models, all considered observables seem more or less to lead to similar growth patterns and attain similar values for larger n. For comparison, Figure 3 depicts the Lanczos coefficients for all four

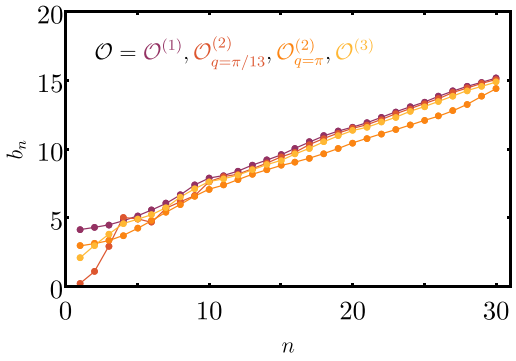

FIG. 3. Comparison between Lanczos coefficients for the Ising model with $B_x = 0.5$ for all four observables considered thus far. The growth is quite similar for larger n hinting at a universality of operator growth.

observables considered thus far for $B_x = 0.5$. This figure certainly supports the hypothesis of a universality of operator growth brought forth in Ref. [14]. Particularly striking is the relation between the observable $O^{(1)}$ and the slow Fourier mode $O^{(2)}_{q=\pi/13}$, since for $n \gtrsim 10$ the coefficients practically coincide.

Before leaving the Ising model and continuing with the Heisenberg model, we want to briefly present data on the 2D Ising model. As the 2D Ising model is nonintegrable, the hypothesis predicts a strict asymptotically linear growth (without logarithmic correction) of the Lanczos coefficients b_n. Respective Hamiltonians of the two-dimensional Ising model are given by

$$\begin{aligned}\mathcal{H}_0 &= \sum_{\ell,\ell'} J_{xx}\sigma^x_{\ell,\ell'}\sigma^x_{\ell+1,\ell'} + J'_{xx}\sigma^x_{\ell,\ell'}\sigma^x_{\ell,\ell'+1} + B_z\sigma^z_{\ell,\ell'},\\ \mathcal{H} &= \mathcal{H}_0 + B_x\sum_{\ell,\ell'}\sigma^x_{\ell,\ell'},\end{aligned} \tag{20}$$

where primed indices number the vertical direction and unprimed indices the horizontal direction.

As in the one-dimensional case, we set $J_{xx} = 1.0$, $B_z = -1.05$, and vary B_x. The coupling strength in the vertical direction is set to $J'_{xx} = 0.5$. Note that this model is nonintegrable for all values of B_x. The energy scale is given by $\mathcal{E} = 3.9$ (for $B_x = 0.5$).

We again consider a local observable whose support is only on one site, i.e.,

$$O = \sigma^x_{0,0}. \tag{21}$$

The Lanczos coefficients b_n are depicted in Fig. 4. Since the space of operators grows extremely fast, it is only practically possible to calculate about 13 coefficients. These coefficients grow in a nicely linear fashion for all values of B_x, which is in accord with the operator growth hypothesis. The coefficients $\mathcal{B}_n$ from the derived upper bound on the moments are so far off that there is an additional vertical axis for the coefficients $\mathcal{B}_n$ on the right side in Fig. 4, which includes a factor of 4. As mentioned, the number N_{sum} is computed iteratively. For the two-dimensional Ising model, the operator space grows so fast that the $\mathcal{B}_n$ are only attainable up to $n = 5$.

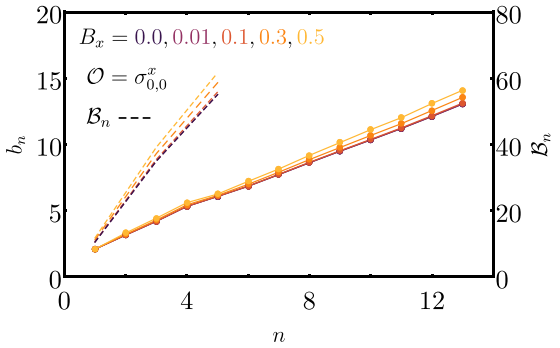

FIG. 4. Lanczos coefficients b_n of the two-dimensional transverse Ising model for an observable $O = \sigma^x_{0,0}$ for various B_x. For all values of B_x the growth is nicely linear. Dashed lines serve as a guide to eye for the coefficients $\mathcal{B}_n$, which are much larger (note the additional vertical axis on the right).

Summarizing the results from this section, the operator growth hypothesis is supported by (most of) the numerical data. The Lanczos coefficients of the one-dimensional nonintegrable Ising models seem to eventually attain approximate linear growth for observables that are local in the fermionic picture. In these cases, the transition from free to nonintegrable is clearly visible. A possible logarithmic correction is not directly noticeable in the presented data. However, it is possible to reveal the predicted correction by rescaling the axes appropriately [17]. Further, the data for the two-dimensional Ising model support the hypothesis for all considered values of B_x. Only the data for the third observable $O^{(3)} = \sigma^x_0$ remain somewhat inconclusive. The transition is not as distinct as for the other observables, however the onset of the hypothesized universal behavior may be suspected for larger n.

All these numerical results support the operator growth hypothesis proposed in Ref. [14] in the sense that the b_n grow asymptotically linear. This is the first main result of the present paper.

The second main result concerns the "maximal" coefficients $\mathcal{B}_n$. While our "optimized" bound in Eq. (14) also corresponds to asymptotically linear growth, there is a significant gap between the $\mathcal{B}_n$ and the actual, physical coefficients b_n.

B. Heisenberg model

The second model of interest is a Heisenberg model with an additional next-nearest-neighbor interaction. Respective Hamiltonians are given by

$$\mathcal{H}_0 = \sum_\ell \sigma^x_\ell \sigma^x_{\ell+1} + \sigma^y_\ell \sigma^y_{\ell+1} + \Delta \sigma^z_\ell \sigma^z_{\ell+1},$$
$$\mathcal{H} = \mathcal{H}_0 + \Delta' \sum_{\ell,\ell'} \sigma^z_\ell \sigma^z_{\ell+2}. \tag{22}$$

The anisotropy of the nearest-neighbor interaction is denoted by Δ, and the integrability-breaking next-nearest-neighbor interaction [28–30] is tuned by the parameter Δ' [which plays the role of λ in Eq. (15)]. The bare Heisenberg chain ($\Delta' = 0$) is integrable for any anisotropy Δ.

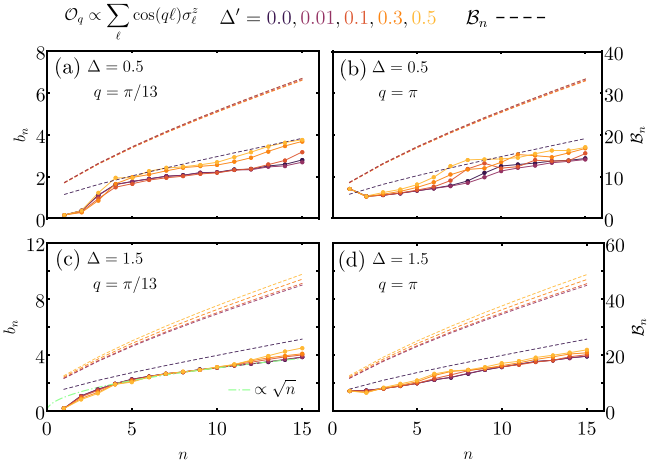

FIG. 5. Lanczos coefficients b_n of the Heisenberg model for spin density waves. Depicted are various combinations of anisotropies and momenta: (a) $\Delta = 0.5$, $q = \pi/13$; (b) $\Delta = 0.5$, $q = \pi$; (c) $\Delta = 1.5$, $q = \pi/13$; (d) $\Delta = 1.5$, $q = \pi$. The integrability-breaking parameter Δ' attains values from 0.0 to 0.5. Dashed lines serve as a guide to the eye for the coefficients $\mathcal{B}_n$, which are much larger (note the additional vertical axes on the right).

The model is gapless and exhibits ballistic transport behavior (of spin and energy) for $|\Delta| < 1$, whereas for $|\Delta| > 1$ the transport of spin is diffusive, while energy transport is still ballistic [31]. In the following numerics, we cover both cases by choosing values $\Delta = 0.5, 1.5$. The parameter Δ' that breaks the integrability is varied in the same fashion as B_x in the Ising model.

Note that the full Hamiltonian in Eq. (22) conserves the total magnetization in the z-direction. Therefore, it is natural to consider spin density waves with momentum q, i.e.,

$$O_q \propto \sum_\ell \cos(q\ell)\sigma^z_\ell. \tag{23}$$

Similar to the energy density wave in the Ising model, we study a relatively slow dynamic with $q = \pi/13$ [depicted in Figs. 5(a) and 5(c) for $\Delta = 0.5, 1.5$, respectively] and a relatively fast dynamic with $q = \pi$ [depicted in Figs. 5(b) and 5(d) for $\Delta = 0.5, 1.5$, respectively].

Since the Heisenberg Hamiltonian contains more coupling terms than the Ising Hamiltonian, the dimension of the operator space (with respect to the Pauli basis) grows faster and we are restricted to a smaller number of coefficients, only about 15.

Comparing the variance (relative deviations) of the Lanczos coefficients for $\Delta = 0.5$ and 1.5, it is striking that the coefficients for $\Delta = 1.5$ vary much less for different values of Δ'. This is most likely due to the relative strength of the perturbation. Let $||\mathcal{H}_0^\Delta||$ denote the norm of the unperturbed Hamiltonian with anisotropy Δ, and $||\lambda\mathcal{V}||$ the strength of the perturbation (where λ conforms to Δ'). Then, for example, $||0.5\mathcal{V}||/||\mathcal{H}_0^{1.5}|| = 0.34$, but $||0.5\mathcal{V}||/||\mathcal{H}_0^{0.5}|| = 0.47$ (for comparison, in the one-dimensional Ising model $||0.5\mathcal{V}||/||\mathcal{H}_0|| = 0.28$). Again, the stronger the perturbation, the faster the coefficients grow, which is simply due to additional terms in the Hamiltonian (in order to not obscure

the main points, we refrain from rescaling the Hamiltonian accordingly). Other than that, the growth is more irregular than in the Ising model, at least in the regime where data are available. For both values of Δ the transition occurs between an integrable ($\Delta' = 0$) and nonintegrable ($\Delta' \neq 0$) model. However, for $\Delta = 0.5$ there is neither visible square-root-like growth in the integrable case nor visible linear growth in the nonintegrable case [for both modes with $q = \pi/13$ in Fig. 5(a) and $q = \pi$ in Fig. 5(b)]. For $\Delta = 1.5$, $\Delta' = 0.0$, and $q = \pi/13$, the growth of the coefficients is more similar to a square root (see the fit) and only visibly deviates for $n \gtrsim 12$; see Fig. 5(c). For the faster mode with $q = \pi$, the growth seems more linear with relatively small deviations; see Fig. 5(d).

The coefficients $\mathcal{B}_n$ are much larger than any of the b_n such that the additional vertical axes contain a factor of 5 in all cases. The number of terms in the sum N_{sum} grows quite a lot faster than in the Ising model due to the next-nearest-neighbor interaction. These terms must in principle be included as soon as Δ' attains an arbitrarily small value strictly greater than zero. This leads to a somewhat gross overestimation, since the energy scale $\mathcal{E}$ remains basically unaltered for small Δ'. This is visible in all figures for the Heisenberg model, where the coefficients $\mathcal{B}_n$ for $\Delta' = 0$ are calculated with the smaller numbers N_{sum} of nearest-neighbor interaction. In principle, one could improve the upper bound on the moments by introducing a second energy scale $\mathcal{E}_{\text{nnn}}$ of the next-nearest-neighbor interaction and count terms according to the appearance of nearest-neighbor terms $\ell_{k,k+1}$ and next-nearest-neighbor terms $\ell_{k,k+2}$. This is, however, more complicated and not in the spirit of the derivations presented in Refs. [14,19].

Summarizing, the numerical data for all considered values of Δ and q can neither really reject nor support the operator growth hypothesis (not least because data for larger n are not available). The transitions between integrable and nonintegrable models are certainly less striking than for the Ising model. Again, only looking at the b_n it would be impossible to say which coefficients belong to an integrable or nonintegrable model. This possibly raises the question of whether the distinction between integrability and nonintegrability regarding the growth of the b_n is an adequate distinction to make. As mentioned in Sec. II, the Lanczos coefficients are uniquely determined by the autocorrelation function $C(t)$. The Heisenberg model for $\Delta = 1.5$ and $\Delta' = 0$ is integrable and exhibits diffusive transport behavior [31], which is usually attributed to chaotic, nonintegrable systems. In view of this, it may not be too surprising that the operator growth hypothesis is not supported by the (limited) numerical data presented in this section. This is the third main result of this paper.

V. CONCLUSION

The first main message of the present paper concerns the explicitly calculated numerical data on the Lanczos coefficients. We numerically probed the universal operator growth hypothesis proposed in Ref. [14], which states that in generic, nonintegrable systems the Lanczos coefficients grow asymptotically linear (with a logarithmic correction in one dimension). We explicitly calculated Lanczos coefficients b_n for various combinations of models (including 1D and 2D Ising models as well as ballistic and diffusive Heisenberg models) and observables (including energy and spin density waves as well as local ones).

We found that the Ising model data generally support the operator growth hypothesis. In particular, as soon as an integrability-breaking perturbation is added to the Hamiltonian, the coefficients eventually attain a linear growth [this transition is more pronounced in the case of a free Hamiltonian with a local observable (in the fermionic picture) than in the case of a free Hamiltonian with a nonlocal observable (in the fermionic picture)]. Further, the two-dimensional Ising model exhibits clear linear growth. The data for the Heisenberg model, however, remain inconclusive. For none of the combinations of considered parameters is there a clear distinction between the integrable and nonintegrable cases. Of course, it may be possible that the hypothesized universal behavior only sets in at some larger n, which is not accessible by our numerical tools.

The second main message of this paper concerns the coefficients $\mathcal{B}_n$, which are obtained by considering the fastest growing moments and converting them into Lanczos coefficients. The physical coefficients b_n seem to grow in a manner that is compatible with the "functional form" of the maximal growth $\mathcal{B}_n$, i.e., we observe more or less linear growth for the Ising models, only with a flatter slope than would be induced by the bound on the moments. Along this line of thinking, there are arguments that suggest that the coefficients $\mathcal{B}_n$ capture the correct asymptotic behavior, only with a rescaled "effective" energy scale $\tilde{\mathcal{E}}$ that is generally different from $\mathcal{E}$ [23]. Thus, treating $\mathcal{E}$ in Eq. (12) as a fitting parameter may give reasonable results. This is, however, beyond the scope of this work, but it is a possible prospect for future research.

ACKNOWLEDGMENTS

We thank D. Parker for interesting discussion on this topic and for a comment on an earlier version of this paper. We are also grateful to A. Dymarsky and J. D. Noh for some helpful remarks and for bringing our attention to related work. This work was supported by the Deutsche Forschungsgemeinschaft (DFG) within the Research Unit FOR 2692 under Grant No. 397107022 (GE 1657/3-2).

APPENDIX: TRANSLATING BETWEEN b_n AND μ_{2n}

For completeness, we briefly present the relation between the Lanczos coefficients b_n and the moments μ_{2n} [32].

(i) *From moments to Lanczos coefficients*: To calculate the Lanczos coefficients b_n from a given set of moments μ_{2n}, we proceed as follows: we define $c_n = \mu_{2n}/\mu_0$ and compute determinants of certain matrices constructed from the normalized moments c_n, i.e.,

$$B_n = \det(c_{i+j})_{0 \leqslant i,j \leqslant n-1}, \tag{A1}$$

where $n \geqslant 2$ and $B_0 = B_1 = 1$, as well as

$$C_n = \det(c_{i+j+1})_{0 \leqslant i,j \leqslant n-1}, \tag{A2}$$

where $n \geqslant 1$ and $C_0 = 1$. Then the Lanczos coefficients are obtained as fractions of determinants via

$$b_{2n}^2 = \frac{B_{n+1}C_{n-1}}{B_n C_n}, \quad b_{2n-1}^2 = \frac{B_{n-1}C_n}{B_n C_{n-1}}. \tag{A3}$$

(ii) *From Lanczos coefficients to moments*: We take the representation L of the Liouvillian $\mathcal{L}$ in the Krylov subspace spanned by the vectors generated by the Lanczos algorithm; cf. Eq. (3). The moments μ_{2n} can be easily read off as the upper-left element of even powers $2n$ of the matrix L, i.e.,

$$\mu_{2n} = (L^{2n})_{00}. \tag{A4}$$

[1] C. Gogolin and J. Eisert, Equilibration, thermalisation, and the emergence of statistical mechanics in closed quantum systems, Rep. Prog. Phys. **79**, 056001 (2016).

[2] J. M. Deutsch, Quantum statistical mechanics in a closed system, Phys. Rev. A **43**, 2046 (1991).

[3] M. Srednicki, Chaos and quantum thermalization, Phys. Rev. E **50**, 888 (1994).

[4] L. D'Alessio, Y. Kafri, A. Polkovnikov, and M. Rigol, From quantum chaos and eigenstate thermalization to statistical mechanics and thermodynamics, Adv. Phys. **65**, 239 (2016).

[5] S. Lloyd, Pure state quantum statistical mechanics and black holes, Ph.D. thesis, Rockefeller University, 1988, arXiv:1307.0378.

[6] S. Goldstein, J. L. Lebowitz, R. Tumulka, and N. Zanghì, Canonical Typicality, Phys. Rev. Lett. **96**, 050403 (2006).

[7] P. Reimann, Typicality for Generalized Microcanonical Ensembles, Phys. Rev. Lett. **99**, 160404 (2007).

[8] C. W. von Keyserlingk, T. Rakovszky, F. Pollmann, and S. L. Sondhi, Operator Hydrodynamics, OTOCs, and Entanglement Growth in Systems without Conservation Laws, Phys. Rev. X **8**, 021013 (2018).

[9] A. Nahum, S. Vijay, and J. Haah, Operator Spreading in Random Unitary Circuits, Phys. Rev. X **8**, 021014 (2018).

[10] T. Rakovszky, F. Pollmann, and C. W. von Keyserlingk, Diffusive Hydrodynamics of Out-of-Time-Ordered Correlators with Charge Conservation, Phys. Rev. X **8**, 031058 (2018).

[11] V. Khemani, A. Vishwanath, and D. A. Huse, Operator Spreading and the Emergence of Dissipative Hydrodynamics under Unitary Evolution with Conservation Laws, Phys. Rev. X **8**, 031057 (2018).

[12] S. Gopalakrishnan, D. A. Huse, V. Khemani, and R. Vasseur, Hydrodynamics of operator spreading and quasiparticle diffusion in interacting integrable systems, Phys. Rev. B **98**, 220303(R) (2018).

[13] A. Chan, A. De Luca, and J. T. Chalker, Solution of a Minimal Model for Many-Body Quantum Chaos, Phys. Rev. X **8**, 041019 (2018).

[14] D. E. Parker, X. Cao, A. Avdoshkin, T. Scaffidi, and E. Altman, A Universal Operator Growth Hypothesis, Phys. Rev. X **9**, 041017 (2019).

[15] D. C. Mattis, How to reduce practically any problem to one dimension, in *Physics in One Dimension* (Springer, Berlin, 1981), pp. 3–10.

[16] V. S. Viswanath and G. Müller, *The Recursion Method: Applications to Many-Body Dynamics* (Springer, New York, 2008).

[17] J. D. Noh, Operator growth in the transverse-field Ising spin chain with integrability-breaking longitudinal field, Phys. Rev. E **104**, 034112 (2021).

[18] A. Dymarsky and M. Smolkin, Krylov complexity in conformal field theory, Phys. Rev. D **104**, L081702 (2021).

[19] D. A. Abanin, W. De Roeck, and F. Huveneers, Exponentially Slow Heating in Periodically Driven Many-Body Systems, Phys. Rev. Lett. **115**, 256803 (2015).

[20] D. S. Lubinsky, An update on orthogonal polynomials and weighted approximation on the real line, Acta Appl. Math. **33**, 121 (1993).

[21] A. Magnus, Asymptotic behaviour of continued fraction coefficients related to singularities of the weight function, in *The Recursion Method and Its Applications* (Springer, Berlin, 1987), pp. 22–45.

[22] X. Cao, A statistical mechanism for operator growth, J. Phys. A **54**, 144001 (2021).

[23] A. Avdoshkin and A. Dymarsky, Euclidean operator growth and quantum chaos, Phys. Rev. Research **2**, 043234 (2020).

[24] P. Mazur, Non-ergodicity of phase functions in certain systems, Physica **43**, 533 (1969).

[25] J. Dehaene and B. De Moor, Clifford group, stabilizer states, and linear and quadratic operations over GF(2), Phys. Rev. A **68**, 042318 (2003).

[26] In Ref. [14], Appendix F, a different upper bound on the moments [similar to the bound in Eq. (14)] is derived, i.e., $\mu_{2n} \leqslant P_n^2 (2\mathcal{E}')^{2n}$, where $P_n \leqslant n4^n \max_{\ell \in [0,n]} \ell^{n-\ell}$ and $\mathcal{E}' = ||h||$. It is shown that this bound corresponds to asymptotically linear growth with a logarithmic correction. Since the spectral function $\Phi(\omega)$ attains negative values for moments equal to the right-hand side of the above bound, it is not possible to obtain corresponding $\mathcal{B}_n$. However, the numbers P_n grow rapidly, much quicker than the sequence of numbers found at the end of Sec. III, and furthermore $2\mathcal{E}'$ is larger than $\mathcal{E}$. Thus, the above bound on the moments is looser than the derived bound in Eq. (14).

[27] M. H. Lee, Ergodic Theory, Infinite Products, and Long Time Behavior in Hermitian Models, Phys. Rev. Lett. **87**, 250601 (2001).

[28] R. Steinigeweg, J. Herbrych, and P. Prelovšek, Eigenstate thermalization within isolated spin-chain systems, Phys. Rev. E **87**, 012118 (2013).

[29] J. Richter, F. Jin, H. De Raedt, K. Michielsen, J. Gemmer, and R. Steinigeweg, Real-time dynamics of typical and untypical states in nonintegrable systems, Phys. Rev. B **97**, 174430 (2018).

[30] M. Rigol and L. F. Santos, Quantum chaos and thermalization in gapped systems, Phys. Rev. A **82**, 011604(R) (2010).

[31] B. Bertini, F. Heidrich-Meisner, C. Karrasch, T. Prosen, R. Steinigeweg, and M. Žnidarič, Finite-temperature transport in one-dimensional quantum lattice models, Rev. Mod. Phys. **93**, 025003 (2021).

[32] C. G. Joslin and C. G. Gray, Calculation of transport coefficients using a modified Mori formalism, Mol. Phys. **66**, 757 (1989).